Degradation of dead cladoceran zooplankton and their contribution to organic carbon cycling in stratified lakes: field observation and model prediction

Aleksandr P. Tolomeev[1,2], Olga P. Dubovskaya[1,2], Georgiy Kirillin[3], Zhanna Buseva[4], Olesya V. Kolmakova[1,2,*], Hans-Peter Grossart[5,6], Kam W. Tang[7], Michail I. Gladyshev[1,2]

[1] Institute of Biophysics, Siberian Branch of the Russian Academy of Sciences, Federal Research Center "Krasnoyarsk Science Center SB RAS", Krasnoyarsk, Russia

[2] Siberian Federal University, Krasnoyarsk, Russia

[3] Department of Ecohydrology, Leibniz-Institute of Freshwater Ecology and Inland Fisheries, Berlin, Germany

[4] Scientific and Practical Center of the National Academy of Sciences of Belarus for Bioresources, Minsk, Belarus

[5] Department of Plankton and Microbial Ecology, Leibniz-Institute of Freshwater Ecology and Inland Fisheries, Neuglobsow, Germany

[6] Institute for Biochemistry and Biology, Potsdam University, Potsdam, Germany

[7] Department of Biosciences, Swansea University, Swansea, United Kingdom

***Corresponding author: kolmoles@ibp.krasn.ru**

KEYWORDS: zooplankton carcasses; non-predatory mortality; sinking velocities; microbial degradation; Lake Stechlin; simulation modeling

Abstract

The contribution of dead zooplankton biomass to carbon cycle in aquatic ecosystems is practically unknown. Using abundance data of zooplankton in water column and dead zooplankton in sediment traps in Lake Stechlin, an ecological-mathematical model was developed to simulate the abundance and sinking of zooplankton carcasses and predict the related release of labile organic matter (LOM) into the water column. We found species-specific differences in mortality rate of the dominant zooplankton: *Daphnia cucullata, Bosmina coregoni,* and *Diaphanosoma brachyurum* (0.008, 0.129 and 0.020 d^{-1}, respectively) and differences in their carcass sinking velocities in metalimnion (and hypolimnion): 2.1 (7.64), 14.0 (19.5) and 1.1 (5.9) m d^{-1}, respectively. Our model simulating formation and degradation processes of dead zooplankton predicted a bimodal distribution of the released LOM: epilimnic and metalimnic peaks of comparable intensity, ca. 1 mg DW m^{-3} d^{-1}. Maximum degradation of carcasses up to ca. 1.7 mg DW m^{-3} d^{-1} occurred in the density gradient zone of metalimnion. LOM released from zooplankton carcasses into the surrounding water may stimulate microbial activity and facilitate microbial degradation of more refractory organic matter; therefore, dead zooplankton are expected to be an integral part of water column carbon source/sink dynamics in stratified lakes.

Introduction

In aquatic ecosystems, decaying organic matter (both autochthonous and allochthonous) including "necromass" resulting from non-consumptive mortality of plants and animals, is considered to be a functionally important part of the carbon cycle (Benbow *et al.*, 2019; Benbow *et al.*, 2020) but the contribution of non-consumptive mortality to carbon fluxes is rarely quantified (Benbow *et al.*, 2020). In lentic ecosystems, zooplankton carcasses, which form "lake snow", represent a large portion of the decaying organic matter (Grossart and Simon, 1998; Benbow *et al.,* 2020). However, zooplankton carcasses are often overlooked as a vector of carbon sequestration (Halfter *et al.*, 2021).

In general, zooplankton bodies contain high-quality substrates, i.e., proteins, lipids and carbohydrates, while the less labile chitin comprises only ca. 7% of the body mass (Błędzki and Rybak, 2016). A recent study showed that labile dissolved organic matter (DOM) released by zooplankton carcasses contained over 7,000 compounds, many of which were N- and S- rich (Johnston *et al.*, 2021). In freshwater habitats, dead zooplankton account for an average of 7.4 – 47.6% of the total zooplankton population (Tang *et al.*, 2014), making zooplankton carcasses a ubiquitous and potentially abundant source of organic carbon, including labile organic matter (LOM). This LOM, released by dead zooplankton, can improve bacterial utilization of recalcitrant organic matter (water humus), including that of terrestrial origin by interactive ("priming") effects (Kolmakova *et al.*, 2019; Neubauer *et al.*, 2021).

There has been an increasing effort to understand the dynamics of zooplankton carcasses in salt- and freshwaters (Tang *et al.*, 2006a; Tang *et al.*, 2009; Tang *et al.*, 2014; Giesecke *et al.*, 2017; Dubovskaya *et al.*, 2018; Kolmakova *et al.*, 2019; Tang *et al.,* 2019; Silva *et al.*, 2020; Daase and Søreide, 2021; Halfter *et al.*, 2021; Neubauer *et al.*, 2021, Diniz *et al.*, 2021). The abundance of zooplankton carcasses is determined by the balance of their production and removal mainly due to sinking and microbial degradation and to a lesser extent ingestion (Elliott et al., 2010; Tang *et al.*, 2014; Daase *et al.,* 2014; Halfter *et al.*, 2021). The sinking rates determine how long zooplankton carcasses will remain in the water column and thus how much they will be degraded, and in what depth the maximum release of carcass organic matter occurs. In stratified lakes, the localization of increased LOM input from dead zooplankton in specific water layers, i.e., density layers such as the pycnocline, may determine the extent that interactive effects increase microbial DOM utilization, particularly of low-bioavailable terrestrial DOM.

In stratified temperate lakes, for example, the water column is divided into epi-, meta- and hypolimnion, each with distinct biological and physicochemical features, such as microbial community compositions (Grossart and Simon, 1998; Simon *et al.*, 2002; Yue *et al.*, 2021; Rojas-

Jimenez *et al.*, 2021), nutrient concentrations, temperature, turbulence, light, pH and dissolved oxygen (Wetzel, 2001). Yet, how these layers may differ in DOM degradation as stimulated by interactive effects remains unclear due to the fact that the effects are often difficult to measure *in situ* and may vary widely according to the lake's characteristics (Bengtsson *et al.*, 2018; Wologo *et al.*, 2021).

The epilimnion has the highest rates of primary production, providing bacteria with labile substrates, and the relatively high temperature and illumination can accelerate organic matter mineralization (Moran and Zepp, 1997; Tranvik and Bertilsson, 2008; Aarnos *et al.*, 2012; Fonvielle *et al.*, 2021). The metalimnion often exhibits increased microbial activities in association with the oxygen minimum zone (Schram and Marzolf, 1994; Kreling *et al.*, 2017). The metalimnic temperature is still high enough to support rapid microbial growth, and the proximity to the hypolimnion provides heterotrophs with limiting nutrients. In addition, the metalimnion receives a high input of fresh organic particles, including zooplankton carcasses, settling from the epilimnion, which accumulate at the pycnocline and sustain high microbial activities there (Grossart and Simon, 1998; Simon *et al.*, 2002). Thus, LOM derived from zooplankton carcasses in the epi- and metalimnion may stimulate microbial activities and hence overall interactive effects on allochthonous carbon cycling in these layers.

The fluxes of zooplankton carcasses within the water column largely depend on physical (e.g., turbulence and sinking velocity) and chemical (pH, oxygen and nutrient availability) variables, but also biological variables (e.g., food web dynamics, zooplankton community composition, mortality rates and habitat depth) (reviewed in Tang *et al.*, 2014). For example, increased turbulence in the epilimnion increases the probability that zooplankton carcasses remain in a given water layer for a prolonged time period (Kirillin *et al.*, 2012); hence, the carcasses may be subject to increased microbial degradation (Tang *et al.*, 2006a; Tang *et al.*, 2009). Once they have reached the metalimnion, the carcasses leave the turbulence zone and begin to sink rapidly and continue through the hypolimnion, where microbial degradation is expected to occur at a much lower rate due to the lower water temperature. Thus, individual lake features would determine the fraction of organic matter that is microbially degraded or remains on the zooplankton carcasses when settling to the hypolimnion and finally being deposited in the sediments, i.e., contribute to carbon sequestration.

To understand the dynamics of the dead zooplankton pool in a stratified lake, sinking and degradation of natural zooplankton carcasses throughout the water column of Lake Stechlin (Germany) were investigated. Based on the studied dynamics in vertical distribution, mortality and sinking rates of the dominant zooplankton species, a simulation model summarizing the contributions of individual species was developed in order to calculate intensity profile of LOM

from dead zooplankton throughout the stratified water column. The results of our field and modeling study advance our understanding of the role of dead zooplankton in microbial organic matter degradation and transformation.

Method

Study site

Lake Stechlin (53°10' N, 13°02' E) is a deep dimictic oligo-mesotrophic lake in northeastern Germany (Koschel and Adams, 2003) which is characterized by an area of 4.23 km^2, a mean depth of 23.3 m, a maximum depth of 69.5 m. Lake Stechlin is thermally stratified from April until the end of December. In 2015- 2017, the lake showed anshowed a strong increase in total phosphorus to 33 $\mu g\ L^{-1}$ and annual mean chlorophyll-a concentration in surface waters to 3.3 $\mu g\ L^{-1}$ (Scholtysik et al., 2020), which altered its trophic status between the mesotrophic and eutrophic states. Changes in phytoplankton and zooplankton biomass revealed the proliferation of cyanobacteria and the decrease of large-sized zooplankton (*Eudiaptomus*, *Eurytemora*) (Selmeczy *et al.,* 2019). Aside of the basic physical, chemical and biological parameters, the *in situ* live-dead zooplankton composition (Bickel *et al.*, 2009), microbial zooplankton carcass decomposition (Tang *et al.*, 2006a, 2009) and non-predatory mortality of *Bosmina longirostris* (O.F. Müller, 1776) (Dubovskaya *et al.*, 2015) have been investigated in detail. Our study was conducted on 27th July – 1st August 2017 at a 20 m deep sampling point in the south-western basin (Fig. 1).

Sediment traps and water column sampling

The methods were similar to our previous field experiments estimating zooplankton non-predatory mortality rate (Dubovskaya *et al.*, 2015; Dubovskaya *et al.*, 2018) with the same accuracy and precision of sampling and trap performance. We used custom-made sediment traps of the Håkanson (1984) type, which consisted of a pair of cylindrical collectors without lids (each cylinder was 0.077 m in diameter × 0.485 m height). We deployed three sets of 2 sediment traps (at 7.0 ± 0.5 m and 14.0 ± 0.5 m depths) for 24 h each of five consecutive days during the summer stratification period in late July - early August 2017. Each set of traps was moored to an anchor and a submerged buoy, which was marked by a small float. Before deployment, the trap cylindrical collectors were filled with water from the corresponding deployment depth pre-screened through a 90-µm mesh. Upon trap retrieval, water from the paired collectors of each trap was pooled and concentrated on a 90-µm mesh. Zooplankton samples were stained with aniline blue for carcass counting (*Y* in Equation 1; see below).

Zooplankton samples were collected daily near the traps at around 9-10 a.m. with an open-close plankton net (90 μm mesh and mouth of 17 cm dia.) from 5 vertical tows: 0-3, 3-6, 6-9, 9-12, and 12-15 m. Samples from layers of 6-9 m and 12-15 m were used to determine carcass abundance at trap exposure depth (y*) for the upper trap (7 m, epilimnion) and the lower trap (14 m, below thermocline at 8-10 m), respectively.

The carcasses accumulation in sedimentation traps and corresponding abundance at trap exposure depths were measured reliably for all studied cladoceran species except for *Chydorus sphaericus* (O.F. Müller, 1776) in the metalimnion. Positioning the traps in an area of variable live and dead *C. sphaericus* populations (7 m) led to significant uncertainties in determining the average background concentration of carcasses per day and consequently for sinking velocities calculationcalculations. Since field measurements of *C. sphaericus* sinking velocity at 7 m were not reliable, this species was excluded from our model analysis. Yet, taking into account that *C. sphaericus* was not abundant and it amounted to maximal 11% of the total cladoceran biomass, its exclusion should not significantly affect our analysis of the processes of formation, destruction and sinking of zooplankton carcasses in Lake Stechlin.

Staining, counting and biomass calculation

To distinguish between live and dead zooplankton, all zooplankton samples were stained within an hour after collection with water-soluble aniline blue (Bickel *et al.*, 2009) and fixed in 10% formalin. Dominant species were counted and measured under a dissecting microscope. These species were Cladocera *Daphnia cucullata* (Sars, 1862)*, Diaphanosoma brachyurum* (Liévin, 1848)*, Chydorus sphaericus* and *Bosmina coregoni* (Baird, 1857). The copepods *Thermocyclops oithonoides* (Sars, 1863) and *Eurytemora lacustris* (Poppe, 1887) were not counted in the samples since their abundance was negligible in the epi- and metalimnion and increased only below 12 m. For samples with > 500 individuals, random subsamples were examined until at least 50 individuals of the same species were counted.

The biomass of zooplankton was calculated based on a linear size-biomass relationship using power-law formulas (McCauley, 1984). Average sizes were obtained by measuring 200 individuals under an inverted microscope (Nikon, Diaphot 300, Japan).

Sinking velocities and fluxes of zooplankton carcasses

The vertical flux F_h (ind. m^{-2} d^{-1}) of carcasses at the trap exposure depth h was measured by sediment traps as

$$F_h = \frac{Y}{S}, \quad (1)$$

where Y is the number of carcasses accumulated in a sediment trap per day (ind. d^{-1}), $S = 0.0093$ m^2 is the input area of the trap. Sinking velocity of carcasses v_h (m d^{-1}) at the depths of trap exposure was derived from the concentration of carcasses at the exposure depth y_h (ind. m^{-3}) and the calculated vertical flux F_h as

$$v_h = \frac{F_h}{y_h}. \quad (2)$$

A normalized flux of carcasses $\bar{F}_h$ (d^{-1}) to the number of live zooplankton was calculated as

$$\bar{F}_h = \frac{F_h}{\int_0^h N(z)dz}, \quad (3)$$

where z is the depth over the layer $0 < z < h$, N is the abundances of live individuals derived from plankton net tows. If the settling carcasses are not destroyed in the water column, then their normalized flow should be the same at all depths. However, if the normalized flux decreases with depth, then this indicates the process of destruction of carcasses within the strata, which has to be considered when modeling zooplankton mortality and LOM release. It is worth noting that the value of the normalized flux is an integral value that depends only on the specific mortality and the number of live zooplankton in the water column above the trap. In the steady state, the flux is not related to the number of dead zooplankton in the water column or to the form of their vertical distribution.

Model of formation, sinking, microbial degradation and destruction of dead zooplankton

The model was constructed to calculate the amount of LOM release by carcasses into the water column. The model is modified from the one used to calculate the vertical distribution of live and dead copepod *Arctodiaptomus salinus* (Daday, 1885) in Lake Shira (Tolomeev *et al.*, 2018), by adding the depth dependence of carcass sinking rate and microbial degradation.

It is assumed that the total amount and the vertical distribution of live zooplankton do not change significantly over time. Its vertical distribution is approximated by k layers of thickness Δz, with corresponding positions $\Delta z \leq z_i \leq k \cdot \Delta z$ and piecewise-homogeneous zooplankton abundances N_i, with $i = 1$ to k. Dynamics of the carcass abundance for the i-th layer is described by the stationary equation for vertical advection with a zero-order source (carcasses production) term and a first-order removal (carcasses destruction) term:

$$\frac{\partial v(z)y_i}{\partial z} = mN_i\delta(z-z_i) - D(z)y_i, \quad (4)$$

where y and N are abundances of carcasses and live individuals (ind. m^{-3}), respectively; m (d^{-1}) is the specific non-predatory mortality, $v(z)$ is the depth-depended sinking velocity of carcasses (m d^{-1}), $D(z)$ is the depth-specific rate of carcass removal or destruction rate (d^{-1}). Here, $\delta(x)$ is the unit sample function defined as

$$\delta(x) = \begin{cases} 1 & \text{if } x < 0 \\ 0 & \text{otherwise} \end{cases}.$$

By definition, $F = v(z)y$ is the vertical flux of carcasses. The solution of Eq. (4) can be written as,

$$y_i(z) = \delta(z - z_i)\frac{mN_i}{D_i}\left(1 - e^{-\frac{D_i}{v_i}\Delta z}\right) + [1 - \delta(z - z_i)]y_{i,z_i}e^{-\int_{z_i}^{z}\frac{D(z)}{v(z)}dz} \cdot \frac{v(z)}{v_i}. \quad (5)$$

The integrated distribution of the carcass concentrations y(z) depicts the sum of the solutions y_i:

$$y(z) = \sum_{i=1}^{k} y_i(z). \quad (6)$$

The important factor that influences the rate of carbon cycling in the water column is the release of LOM by sinking zooplankton carcasses. We separated the model parameterization of the LOM release rate (μg DW m^{-3} day^{-1}) in two processes with different time scales: the "microscale" $I_{DW\rho}(z)$ describes the slow and continuous loss of density due to continuous release of organic matter by microbial degradation, while the "macroscale" $I_D(z)$ represents the mechanical fragmentation of carcasses (the stage of entire carcasses disappearance, suggesting their quick degradation). The amount of LOM released by a carcass is proportional to the change in its density. The density ρ_o corresponds to the initial body weight of the zooplankter $DW\rho_0$ (μg), and the lower limit density $\rho_{term} = 1000$ kg m^{-3} corresponds to its complete destruction; i.e., the density at which the amount of LOM released into the medium is equivalent to the entire body weight of the zooplankter. The weight of the carcass, depending on ρ, is determined by the formula:

$$DW\rho = DW\rho_0 \cdot \frac{\rho - \rho_{term}}{\rho_0 - \rho_{term}} \quad (7).$$

Elliott *et al.* (2010) proposed the empirical equation describing the carcass density dependence on time and temperature:

$$\rho = \rho_o - 3.78 \cdot (1 - e^{-0.329T}) \cdot (\ln(t) + 1.39), \quad (8)$$

where $\rho_o = \rho(0.25) = 1045$ is the initial carcass density (kg m^{-3}), T - temperature (°C) and t – time after death (from 0.25 h onward). Ranging from t = 0 to t = 0.25 h, the density ρ is not defined, therefore, we will assume that the density of carcasses does not change in the first 0.25 hours after animal death.

According to Equation 8, the most intense release of LOM occurs within the first hours after death (logarithmic dependence on time). Zooplankton carcasses within the water column consist of carcasses that have different "ages" from the moment of death and therefore have different rates of LOM release; therefore, to calculate the LOM profile, it is necessary to know not only the total number of carcasses, but also their "age" structure in each layer.

The rate of release of LOM from zooplankton carcasses can be determined based on the obtained i-solutions $y_i(z)$ by Equation 5, reflecting the total number and the "age" structure of dead zooplankters. Let us denote the rate of LOM release in the i-solution associated with changes in carcasses' density as $I_{DW\rho_i}(y_i, z)$, whose vertical profile is defined as:

$$I_{DW\rho}(z) = \sum_{i=1}^{k} I_{DW\rho_i}(y_i, z) \qquad (9)$$

We will find the vertical distributions $I_{DW\rho_i}$ as discrete values of the LOM release rate in layers $\boldsymbol{z}_{i+n}$, where n is an integer $0 \leq n \leq k - i$. The LOM flux in layer $\boldsymbol{z}_i$, associated with the change in carcass body weight in each i-solution can be described as follows:

$$I_{DW\rho_{i,z_i}} = (DW\rho_0 - DW\rho_{i,z_i}) \cdot y_{i,z_i} \cdot \frac{v_{i,z_i}}{\Delta z} \qquad (10)$$

where $DW\rho_0$ is initial weight of carcass, $DW\rho_{i,z_i}$ is weight of carcass after time $\Delta t_{i,z_i} = \frac{\Delta z}{v_{i,z_i}}$, in which the carcass sinks to the lower boundary of the layer $\boldsymbol{z}_i$. At depth $z > z_i$ the LOM flux is defined as

$$I_{DW\rho_{i,z_{i+n}}} = (DW\,\rho_{i,z_{i+n-1}} - DW\rho_{i,z_{i+n}}) \cdot y_{i,z_{i+n}} \cdot \frac{v_{i,z_{i+n}}}{\Delta z}, \qquad (11)$$

where n is an integer in the range $1 \leq n \leq k - i$. $DW\rho_{i,z_{i+n-1}}$ and $DW\rho_{i,z_{i+n}}$ are the weight of carcasses at the upper and lower boundaries of the layer $\boldsymbol{z}_{i+n}$, respectively. $y_{i,z_{i+n}}$ is the number of carcasses at the depth z_{i+n}, $v_{i,z_{i+n}}$ is the sinking velocity of carcasses in the layer $\boldsymbol{z}_{i+n}$.

Calculation of the LOM flux profile by Equation 11 requires finding $DW\rho$ corresponding to the densities $\rho_{i,z_{i+n-1}}$ and $\rho_{i,z_{i+n}}$ for each water depth. However, Equation 7 does not allow direct estimate of $\rho_i(z)$ at arbitrary water depths below z_i due to the undefined variables $v(z)$ and $T(z)$.

Nevertheless, it is possible to find $\rho_i(z)$ using a recursive procedure calculating $\rho_{i,z_{i+n}}$ from the value on the previous time step $\rho_{i,z_{i+n-1}}$. With the density of carcasses at the upper boundary of the current layer known, the reference time t' can be calculated back to the moment of zooplankter' death assuming constant $v(z) = v_{i,z_{i+n}}$ and $T(z) = T_{i,z_{i+n}}$. We find the time t' by the backward solution of Equation 8 with regard to *t*.

$$t' = \exp\left[\frac{e^{0.329\cdot T}\cdot\left(\rho_0 - \rho_{i,z_{i+n-1}}\right)}{3.78\cdot(e^{0.329\cdot T}-1)} - 1.39\right] \qquad (12)$$

Then, substituting time $(t' + \Delta t_{i,z_{i+n}})$ into equation 8 as *t*, we yield $\rho_{i,z_{i+n}}$, and can repeat the cycle until the lower limit of the simulated depth range is reached. As a result, we can determine all $\rho_{i,z_{i+n}}$ needed to compute $DW\rho_{i,z_{i+n}}$ and thus obtain the depth profile $I_{DW\rho}(z)$ by Equation 9.

Another form of release of organic matter by dead zooplankton is the complete destruction of carcasses, determined by *D(z)* in Equation 4. In this case, the organic matter enters the environment in the form of fragments of crustacean bodies. This type of organic matter can also play an important role in accelerating the carbon cycle of the water column because the particles still contain bacteria and fungi decomposing them in an attached form. The intensity of the release of organic matter $I_D(z)$, determined by the destruction of carcasses, is also calculated based on the sum of *i*-solutions $y_i(z)$ similarly to the equation 9:

$$I_D(z) = \sum_{i=1}^{k} I_{D\,i}(y_i, z). \qquad (13)$$

However, instead of calculating the losses associated with the decrease in carcass weight during their passage through the water layer, it is necessary to determine the difference in carcass numbers entering and leaving the water layer. Multiplying the obtained value by the initial carcass weight in the considered layer and dividing it by the time required for passing the water layer, we obtain value $I_{D\,i}$. In layer $\mathbf{z}_i$ it will be defined as

$$I_{D\,i,z_i} = (m \cdot N_{i,z_i}\, t_{i,z_i} - y_{i,z_i}) \cdot DW\rho_0 \cdot \frac{v_{i,z_i}}{\Delta z}, \qquad (14)$$

and at depth $z > z_i$ as

$$I_{D\,i,z_{i+n}} = (y_{i,z_{i+n-1}} \cdot \frac{v_{i,z_{i+n-1}}}{v_{i,z_{i+n}}} - y_{i,z_{i+n}}) \cdot DW\ \rho_{i,z_{i+n-1}} \cdot \frac{v_{i,z_{i+n}}}{\Delta z}, \qquad (15)$$

here *n* depicts an integer in the range $1 \leq n \leq k - i$.

Use of smoothed zooplankton distributions for the model

Modeling the vertical distribution of dead zooplankton and the resulting LOM flux requires detailed distributions of live and dead zooplankton for each layer z_i as initial input. Distributions of zooplankton were obtained from field observation data. For each day, the distribution data were smoothed by the method of kernel density estimation for heaped and rounded data (Gross, 2015). The obtained profiles of live and dead zooplankters of each species were further used for model calculations.

Specific mortality m *and sinking velocities of carcasses* v(z) *at condition* D(z) ≈ 0.

Laboratory experiments indicate that at 20 °C zooplankton carcasses did not reach the late stage of degradation until ca. 78 hours (3.25 days) after death (Tang *et al.*, 2006b). Consequently, zooplankton species with high sinking rates (~20 m day^{-1}) will have sufficient time to leave the water column before full disintegration. Under these conditions, we can assume $D(z) \approx 0$ that makes possible calculation of the absolute values of m and $v(z)$ in a steady state system by the established formulas (Dubovskaya *et al.*, 2015):

$$m = \frac{y^* \cdot v^*}{\bar{N} \cdot h}\ ,\ v(z) = \frac{m \cdot \bar{N}_z \cdot z}{y(z)} \quad (16)$$

where y^* is carcass concentration at trap depth h , v^* is carcass sinking velocities at trap depth, $\bar{N}$ is averaged abundance of live individuals over the layer $0 < z < h$, $\bar{N}_z$ is averaged concentration of live individuals in the water column from the surface to depth z.

Specific mortality m *and sinking velocities of carcasses* v(z) *at condition* $D(z) \gg 0$.

If the factor depth significantly affects the value of normalized flow $\bar{F}(z)$, then this indicates high rates of carcass removal rate in the water column, and $D(z)$ becomes important for the model. Since the rate of degradation is strongly dependent on temperature, one can expect that in the warmer epilimnion, disintegration of the carcasses will occur more rapidly. However, the carcasses start to break apart only on the late stages of degradation, after the loss of a major portion of their carbon content. The rate of carbon release varies between species, but it usually occurs over several days. For instance, 50% of copepod carcass carbon is mineralized within 6−12 d at a temperature close to 20°C (Franco-Cisterna et al., 2021). In Lake Stechlin, *Daphnia cucullata* carcasses lose 26 to 43% C d^{-1} over a 2-day *in situ* experiment (Tang *et al.*, 2009). Even in the late stage of decomposition when most of the carcasses' internal tissues have disappeared, the chitinous carapace remains relatively intact (Tang *et al.*, 2009). Consequently, despite the high rate of carbon loss by carcasses in the epilimnion, the carcasses even at low rates of sinking (1-2 m d^{-1}) have a high probability to leave the epilimnion before disintegration. Thus, it can be assumed that removal rate

of carcasses in the epilimnion zone is insignificant compared to the lower layers. Therefore, we set D to zero in the upper 7 m of the water column (epilimnion), so that, m and $v(z)$ in the layer 0-7 m can be found from Equation 16.

In order to obtain $D(z)$ below 7 m it is necessary to know $v(z)$ below this depth. For this, we used the sinking velocities of carcasses measured *in situ* at 7 m and 14 m. Denoting $v_{D0}(z)$ as the "reference" sinking velocity at $D(z) \approx 0$, and $z_7 = 7$ m and $z_{14} = 14$ m as the depths corresponding to the measured sinking velocities, the actual sinking rate $v(z)$ passing through z_7 and z_{14} can be approximated linearly as:

$$v(z) = K(z) \cdot v_{D0}(z) \text{ for } z_7 < z < z_{14}, \quad (17)$$

$$K(z) = b + a \cdot z,$$

where b and a are the coefficients of the line passing through $K(z_7) = 1$ and $K(z_{14}) = v_{trap}(z_{14}) / v_{D0}(z_{14})$. Fig. 2 shows an example approximating sinking velocity curve $v(z)$ for *Daphnia* (data collected on 1st August, 2017) assuming $D(z) \gg 0$, passing through the measured sinking velocity point at 14 m. Given the distribution $v(z)$ for $D(z) \gg 0$ in the 7-14 m layer, D can be calculated from Equation 5. It however involves solution of a transcendental equation. As a workaround, we assume that the destruction rate of carcasses produced in each single layer $\boldsymbol{z_i}$ is equal to zero (i.e., in layer $\boldsymbol{z_i}$, only the carcasses degrade, deposited from the upper layers). The assumption is plausible because a newly formed carcass is unlikely to be immediately destroyed. Then the destruction rate D_{z_i} is determined as follows:

$$D_{z_i} \simeq \ln\left(-\frac{y_{i-1} \cdot \frac{v_{i-1}}{v_i}}{m \cdot N \cdot \frac{\Delta z}{v_i} - y_i}\right) \cdot \frac{v}{\Delta z} \quad (18)$$

All model calculations were implemented in the programming language R, ver. 4.1.1 (R Core Team, 2021), using the basic R functions and the tidyverse packages (Wickham *et al.*, 2019). To find the boundaries of the metalimnion, we used the R package rLakeAnalyzer (Winslow *et al.*, 2019).

Results

Vertical distribution in abundance of live and dead zooplankton and carcass sinking flux

Cladocerans dominated the zooplankton community, represented by four main species: *Daphnia cucullata* and *Bosmina coregoni* in the epilimnion; *Diaphanosoma brachyurum* and *Chydorus sphaericus* in the metalimnion (Fig. 3 - 6). Among these, *D. cucullata* and *D. brachyurum*

contributed ca. 50% and 30% of the biomass, respectively (Table 1). The averaged percentages of carcasses among these zooplankton species ranged from 4.6% to 8.9% throughout the water column, 0-15 m (Table 1).

Abundance of live and dead cladocerans in the water column per m^2 varied noticeably during the six days of sampling. However, these fluctuations usually did not exceed a factor of two. An exception was the abundance of live *B. coregoni*, which varied by a factor of 6.5 (Fig. 4 C). The distribution of *D. cucullata* and *B. coregoni* populations within the epilimnion zone was patchy. We observed substantial changes in the abundance of live individuals in different layers of the epilimnion over time (Fig.3 A, 4 A). The dynamics and spatial distribution of metalimnetic populations of *D. brachyurum* and *C. sphaericus* were more consistent (Fig. 5 A, 6 A).

The dynamics of dead and live individuals of *D. cucullata* were closeclosely linked with each other (Fig. 3 A-C). Changes in abundance of carcasses of *B. coregoni* also followed those of living individuals (m^{-2}), except on 31st July (Fig. 4 A-C). However, the dynamics of carcasses of both *D. brachyurum* and *C. sphaericus* differed substantially from live individuals (Fig. 5 A-C and Fig. 6A-C).

Carcass sinking fluxes of *D. cucullata* and *B. coregoni* measured by sediment traps each day were similar at 7 m and 14 m depths, but differed markedly between the sampling time points (Fig.3 D, 4 D). In contrast, the sinking flux of *D. brachyurum* carcasses considerably decreased from 7 m to 14 m (about 2.5 times) (Fig. 5 D). Accumulation of *C. sphaericus* carcasses was also lower in the lower traps (Fig.6 D).

Sinking velocities and normalized fluxes

Distribution of sinking velocities of *B. coregoni*, *D. cucullata*, and *D. brachyurum* at 7 m and 14 m depths, i.e. in tothe meta- and hypolimnion, revealed a similar pattern (Table 1). Sinking velocities of these cladocerans were significantly lower at 7 m than at 14 m. *B. coregoni* carcasses sinking rate was the highest among all species and reached 14 and 20 m d^{-1} at 7 and 14 m depths, respectively. Yet, the increase in *B. coregoni* sinking rate at 14 m was not pronounced (ca. 1.5-fold) when compared to *D. cucullata* and *D. brachyurum* carcasses, which were sinking at 1 - 2 m d^{-1} in the metalimnion, but increased to 6 - 8 m day^{-1} at 14 m depth (Table 1).

Differences in normalized fluxes of *D. cucullata* and *B. coregoni* carcasses between 7 m and 14 m depths were not significant (Table 1), indicating that these carcasses were not substantially degraded in the water column. It is worth noting that the normalized fluxes of *B. coregoni* carcasses (0.110-0.134 d^{-1}) were an order of magnitude higher than those of *D. cucullata*

409 (0.006-0.007 d^{-1}). The decrease in the normalized flux of carcasses of *D. brachyurum* from 0.017 d^{-1}
410 at 7 m to 0.003 d^{-1} at 14 m was significant (Table 1).
411
412 *Simulation results*
413 The non-predatory mortality was highest for *B. coregoni* (0.129 d^{-1}), followed by *D.*
414 *brachyurum* (0.020 d^{-1}) and finally *D. cucullata* (0.008 d^{-1}; see also Table 2). The significantly
415 higher mortality of *B. coregoni* than of other species was consistent with the highest percentage of
416 dead *B. coregoni* in the water column (Table 1).
417 Sinking velocities of dead individuals of these cladoceran species had a similar pattern of
418 vertical distribution (Fig.7). The calculated sinking velocities were minimal in the epilimnion (ca. 1-
419 2 m d^{-1} for *D. cucullata* and *D. brachyurum* and ca. 6-7 m d^{-1} for *B. coregoni*), which is consistent
420 with the higher epilimnic turbulence. From the metalimnion to the hypolimnion, carcass sinking
421 rates increased, but in the deeper part of the hypolimnion they tended to stabilize or even decrease
422 (below 12 m for *B. coregoni* and *D. brachyurum*). Sinking velocity of *D. cucullata* carcasses,
423 however, further increased at 14 m. Yet, accuracy of sinking velocity calculations decreased at
424 lower depths as live and dead zooplankton abundances were relatively low in these water layers. It
425 may seem confusing that carcass sinking velocities near the surface were close to zero. In fact, the
426 model does not show the physical sinking velocity of individual carcasses, but rather the resulting
427 settling and rising velocities of the whole population. For example, if turbulent vortices hold the
428 carcass in the surface layer, the resulting sinking velocity would be indeed low.
429 Although the decrease in normalized carcass fluxes from 7 to 14 m for *D. cucullata* and *B.*
430 *coregoni* was statistically insignificant (Table 1), we assume that the degradation of dead
431 zooplankton in the water column was within our methodological accuracy. Nevertheless, we
432 estimated carcass destruction rates (*D*) assuming a proportional increase in sinking velocities
433 between 7 and 14 m, according to the Eqs. 17 and 18. Maximum destruction rate *D* in the 7 -14 m
434 water layer were 0.36 d^{-1} and 0.71 d^{-1} for *D. cucullata* and *B. coregoni*, respectively, and occurred
435 at the lowest depth, i.e. 14 m (Table 2, Fig.7).
436 For *D. brachyurum*, the normalized carcass flux decreased by as much as 82% between 7
437 and 14 m (Table 1). The large difference between the measured sinking velocity (5.9 m d^{-1}; Table 1)
438 and the calculated velocity (34.9 m d^{-1}; Table 2) at 14 m indicates a high destruction rate of *D.*
439 *brachyurum* carcasses. Our model (without any carcass destruction) and actual sinking velocities of
440 *D. cucullata* and *B. coregoni* carcasses differed only by 1.5 and 1.2 times, respectively, but by
441 almost 6 times for *D. brachyurum* (Table 2). The destruction rate of *D. brachyurum* was estimated
442 to be 3.99 d^{-1}(Table 2).

443 Different species contributed differently both to the formation of total LOM of dead
444 zooplankton, and to its separate fractions I_{DW_ρ} and I_D (Table 2). The largest contribution to LOM
445 as I_{DW_ρ} was made by *B. coregoni* at 3.87 ± 0.42 mg DW m^{-2} (44.3%), due to its high population
446 mortality during the study period and the low rate of carcasses destruction. The highest input of
447 LOM in the form of destroyed carcasses I_D was from *D. brachyurum* at 2.93 ± 0.54 mg DW m^{-2}
448 (62.4 %). *D. cucullata*, despite dominating the biomass (50%) of all cladocerans, contributed
449 relatively little LOM: 2.18 ± 0.13 mg DW m^{-2} (25.6 %) and 0.54 ± 0.15 mg DW m^{-2} (10.1 %) of the
450 fractions I_{DW_ρ} and I_D, respectively, because of its low mortality rate during the observation period.

451 The profile I_{DW_ρ} showed two maxima, one in epilimnion (2.5 m) formed by *B. coregoni*
452 and *D. cucullata*, and one in metalimnion (7.5 m) formed mainly by *D. brachyurum* (Fig. 8). Both
453 maxima were comparable to each other and yielded an input of LOM of 0.7 - 1.2 mg m^{-3} d^{-1}. Since
454 the highest rate of organics released by the crustacean carcasses has been observed in the first few
455 hours after the animal's death, the profile of LOM influx practically coincided with the distribution
456 of carcasses in the water column (Fig. 8). In other words, the carcasses lost most of their organic
457 matter not far from the place of their formation.
458 Total destruction of carcasses I_D began in the metalimnion and reached maximum values of
459 0.8 mg m^{-3} d^{-1} approximately at the bottom of the thermocline at 8 m depth and then gradually
460 decreased with increasing depth. A smooth reduction in I_D was achieved by a balance between
461 some increase in carcass destruction rate with sinking time and the decrease in carcass abundance
462 with depth (Fig. 8).

463

464 **Discussion**

465 We revealed distinct species-specific differences in carcass distribution, sinking and
466 potential release of LOM and microbial degradation in the water column of a stratified lake. In
467 particular, planktonic crustaceans differed in their abundances, mortality rates, sinking velocities,
468 and carcass degradation rates in different water layers, i.e., epi-, meta-, and hypolimnion. We tried
469 to distinguish between the release of organic matter in the beginning and later stages of carcass
470 degradation and relate them to the spatial structure of cladoceran zooplankton using the modeling
471 approach.
472 The analysis of the processes of carcass degradation by means of the model revealed
473 findings that were not obvious. For example, the abundance of *B. coregoni* carcasses was 5 times
474 lower than *D. cucullata* carcasses and it was minimal among all cladoceran species, but the sinking

velocities of *B. coregoni* carcasses were the highest, suggesting a short residence time in the water column. The high sinking velocity of *B. coregoni* carcasses in comparison to all other cladocerans was probably due to their relatively higher body density. *B. coregoni*, which had a body size ca. 1.6 times smaller than *D. cucullata*, nevertheless had almost the same body weight (1.9 µg DW). Therefore, one would expect *B. coregoni* to make a smaller contribution to the total LOM. However, the overall mortality of the *B. coregoni* population was the highest of all species studied, exceeding the mortality of *Daphnia* by ca. 16 times. This compensated for the relatively low abundance of this species and its high carcass sinking velocity, resulting in a large *Bosmina* contribution to the total LOM flow via zooplankton carcasses. The I_{DW_ρ} fraction of LOM released by *B. coregoni* was the highest among all species, at 44 %. The abundance of *D. brachyurum* and *D. cucullata* carcasses were of the same magnitude, but *D. brachyurum* contributed 62% (I_D fraction) compared to 10 % for *D. cucullata* to the total LOM, due to the higher destruction rate and the lower sinking velocity of *D. brachyurum* carcasses.

It is worth noting that non-predatory mortality values can vary over a wide range for natural cladoceran populations from low during growth and steady-state to high during population decline (Gladyshev et al., 2003; Tang et al., 2014). The development conditions for the *B. coregoni* population during the observation period were likely less favorable than for other species. For instance, the non-predatory mortality rate of a closely related species *Bosmina longirostris* derived from sediment trap data in Lake Stechlin during steady-state of the population (Dubovskaya *et al.*, 2015) was lower: 0.015 d^{-1}. However, non-predatory mortality rates of *Daphnia* measured by sediment traps in Lake Constance was of the wide range 0.002–0.18 d^{-1} (Gries and Güde, 1999) as in our study. This suggests that the contribution of zooplankton carcasses to the overall carbon flux and their ability to stimulate microbial organic matter degradation in each period of the growth season was highly species-specific and depended on the current state of the populations and lake ecosystem. In order to calculate the parameters I_{DWp} and I_D of the released LOM, the model has to rely on some assumptions that may need further explanation. One of the most important assumptions made in the model is that there is no significant carcass destruction in the epilimnion. A comparison of the normalized carcass fluxes of *D. cucullata* and *B. coregoni* for the 7 and 14 m water layers shows that their destruction in the upper layers can be indeed neglected. Underestimation of carcass destruction (if any) actually means an underestimation of the non-predatory mortality for the species. However, with fixed sinking velocities, any increase in non-predatory mortality values will lead to an increase in carcass destruction rates at lower depths according to the model. As a result, the correction made may affect the absolute calculated values of natural mortality and thus carcass destruction rates, but does not substantially affect the shape of the vertical profile of LOM release from sinking carcasses. Consequently, our model results concerning

occurrence, relative location, and relative magnitude of LOM released from dead zooplankton throughout the water column will be valid regardless of the assumptions made.

Our model predicts two peaks of organic matter release—one located in the epilimnion and the other one in the metalimnion—both having different origins. The epilimnion peak of LOM release is associated with the mortality of zooplankton primarily inhabiting the upper water layers (e.g. *Daphnia* and *Bosmina*). It is formed by substances released by fresh zooplankton carcasses during the first hours (up to one day) after death while maintaining carapace integrity. In the model, this fraction is defined through the loss of carcass density I_{DW_ρ} and refers to the highly biodegradable carbon fractions in dissolved or partially solid form. This fraction can supply heterotrophs with the energy and nutrients needed to synthesize enzymes capable of degrading less bioavailable material (Neubauer et al., 2021). The deeper metalimnetic peak is associated with carcasses of *D. brachyurum* contributing to a local LOM release I_{DW_ρ} enforced by the flux of organic particles (I_D) from the upper water layers. The latter fraction I_D represents the entry of organic matter into the surrounding medium in form of fragmented carcass particles. Obviously, the LOM fraction represented by I_D is of lesser quality, because of the higher proportion of chitin at the late stages of microbial carcass degradation. However, fragments of the disintegrated carcasses spread into a much larger volume of the water column, carrying attached microorganisms and allowing them to get in contact with other organic particles in the water column. Additionally, smaller particles may have lower excess density and, therefore, can be trapped in the density gradient zone (thermocline) and involved in the local carbon cycle. Chitin, being a relatively hard-to-degrade polysaccharide, still contains nitrogen molecules needed by bacteria. Therefore, under conditions of nitrogen deficiency, it promotes development of specialized heterotrophs that can decompose polysaccharides for nitrogen mining (see e.g. Bengtsson et al., 2018). This increases microbial species diversity, which is necessary for a more effective mineralization of organic matter with a low bioavailability in lakes.

The depth of formation of the second peak corresponds approximately to the depth of 8 m (intersection of curves I_{DW_P} and I_D), which is the bottom of the thermocline. With the observed composition and distribution of zooplankton, the most likely zones of carcass-induced increase in interactive effects as determined by the release of LOM from dead zooplankton are localized either in the epilimnion or in the metalimnion zone, i.e. at the thermocline density gradient.

The predicted zones of maximum LOM release do not necessarily correspond to the highest microbial carbon mineralization rates in the water column (data of Franco-Cisterna et al., 2021), but may represent the starting point for microbial organic matter remineralization and related interactive ("priming") effects (Kolmakova *et al.*, 2019; Neubauer *et al.*, 2021). In any case, our model

provides reliable estimates for scenarios of carcass LOM release and transfer into the surrounding during carcass sinking throughout the stratified water column. It suggests an important role of sinking zooplankton carcasses for the overall lake carbon cycle. Nevertheless, to better quantify their significance, the formation of microbial aggregates and the interactions of carcass LOM with organic material of different origins (e.g. dead phytoplankton and allochthonous particulates) and their hydrophysical properties, i.e. buoyancy and accumulation at density gradients such as the pycnocline, need to be investigated. The accumulation of carcass LOM and other organic matter in distinct water layers as indicated by our model can potentially accelerate microbial mineralization of both autochthonous and allochthonous organic matter and thus profoundly affect the carbon source and sink functions of stratified lakes.

Conclusions

Sinking velocity, mortality rates, and degradation rates of cladoceran carcasses in the stratified lake were species-specific. The model simulation allowed us to describe mechanisms of LOM formation from zooplankton carcasses in a stratified lake and to determine vertical profiles of LOM distribution, which appeared to vary in space and time. The model predicts a bimodal occurrence of LOM release intensity peaks in relation to the presence and sinking of zooplankton carcasses throughout the water column, with epilimnic and metalimnic peaks. The epilimnic LOM peak was primarily formed by microbial LOM release from fresh zooplankton carcasses without destroying carcass integrity. The metalimnic peak, however, comprised of LOM released by both intact, fresh carcasses from the metalimnion but also aged, heavily degraded carcasses from the epilimnion. This carcass LOM mixture potentially increases metalimnic LOM chemodiversity and diversity of the microbial community, and likely intensifies microbial organic matter degradation. Thus, LOM of zooplankton carcasses, in particular when accumulating at density layers such as the pycnocline has the potential to change the carbon sink towards a carbon source function of stratified lakes, which will be further amplified by current global warming.

Acknowledgements

We thank all technicians of IGB department Plankton and Microbial Ecology

Conflict of interest

Authors declare no conflict of interest.

Funding

HPG has been funded via the projects Zooflux (GR1540/29-1) and Pycnotrap (GR1540/37-1) provided by the German Science Foundation (DFG). Funding for MIG was provided by grant of Russian Basic Research Foundation No. 21-54-12003.

References

Aarnos, H., Ylöstalo, P., and Vähätalo, A. (2012) Seasonal phototransformation of dissolved organic matter to ammonium, dissolved inorganic carbon, and labile substrates supporting bacterial biomass across the Baltic Sea. *J. Geophys. Res.: Biogeosci.*, **117**, 1004.

Benbow, M. E., Receveur, J. P., and Lamberti, G. A. (2020) Death and Decomposition in Aquatic Ecosystems. *Front. Ecol. Evol.*, **8**, 17.

Benbow, M. E., Barton, P. S., Ulyshen, M. D., Beasley, J. C., DeVault, T. L., Strickland, M. S., Tomberlin, J. K., Jordan, H. R., *et al*. (2019) Necrobiome Framework for Bridging Decomposition Ecology of Autotrophically and Heterotrophically Derived Organic Matter. *Bull. Ecol. Soc. Am.*, **100**, e01454.

Bengtsson, M. M., Attermeyer, K., and Catalán, N. (2018) Interactive effects on organic matter processing from soils to the ocean: are priming effects relevant in aquatic ecosystems? *Hydrobiologia*, **822**, 1–17.

Bickel, S. L., Tang, K. W., and Grossart, H.-P. (2009) Use of aniline blue to distinguish live and dead crustacean zooplankton composition in freshwaters. *Freshwater Biol.,* **54**, 971–981.

Błędzki, L. A. and Rybak, J. I. (2016) Freshwater crustacean zooplankton of Europe: Cladocera & Copepoda (Calanoida, Cyclopoida) key to species identification, with notes on ecology, distribution, methods and introduction to data analysis. Springer International Publishing.

Daase, M., Varpe, Ø., Falk-Petersen, S. (2014) Non-consumptive mortality in copepods: occurrence of *Calanus* spp. carcasses in the Arctic Ocean during winter. *J. Plankton Res.*, **36**, 129–144.

Daase, M. and Søreide, J. E. (2021) Seasonal variability in non-consumptive mortality of Arctic zooplankton. J. Plankton Res., 43, 565–585.

Diniz, L. P., FranÇa, E. J., Bonecker, C. C., Marcolin, C. R., Melo JÚnior, M. (2021). Non-predatory mortality of planktonic microcrustaceans (Cladocera and Copepoda) in neotropical semiarid reservoirs. *Anais da Academia Brasileira de Ciencias*, **93**.

Dubovskaya, O. P., Tolomeev, A. P., Kirillin, G., Buseva, Z., Tang, K. W., and Gladyshev, M. I. (2018) Effects of water column processes on the use of sediment traps to measure zooplankton non-predatory mortality: a mathematical and empirical assessment. J. Plankton Res., 40, 91–106.

612 Dubovskaya, O. P., Tang, K. W., Gladyshev, M. I., Kirillin, G., Buseva, Z., Kasprzak, P.,
613 Tolomeev, A. P., and Grossart, H.-P. (2015) Estimating In Situ Zooplankton Non-Predation
614 Mortality in an Oligo-Mesotrophic Lake from Sediment Trap Data: Caveats and Reality Check.
615 *PLoS ONE*, **10**, e0131431.
616 Elliott, D. T., Harris, C. K., and Tang, K. W. (2010) Dead in the water: The fate of copepod
617 carcasses in the York River estuary, Virginia. *Limnol. Oceanogr.*, **55**, 1821–1834.
618 Fonvielle, J. A., Giling, D. P., Dittmar, T., Berger, S. A., Nejstgaard, J. C., Lyche Solheim,
619 A., Gessner, M. O., Grossart, H., *et al*. (2021) Exploring the Suitability of Ecosystem Metabolomes
620 to Assess Imprints of Brownification and Nutrient Enrichment on Lakes. *J. Geophys. Res.:*
621 *Biogeosci.*, **126**.
622 Franco-Cisterna, B., Stief, P., and Glud, R. N. (2021) Temperature effects on carbon
623 mineralization of sinking copepod carcasses. *Mar. Ecol.: Prog. Ser.*, 679, 31-45.
624 Giesecke, R., Vallejos, T., Sanchez, M., and Teiguiel, K. (2017) Plankton dynamics and
625 zooplankton carcasses in a mid-latitude estuary and their contributions to the local particulate
626 organic carbon pool. *Cont. Shelf Res.,* **132**, 58–68.
627 Gladyshev M.I., Dubovskaya, O.P., Gubanov, V.G., and Makhutova O.N. (2003) Evaluation
628 of non-predatory mortality of two Daphnia species in a Siberian reservoir. *J. Plankton Res*., 25,
629 999-1003.
630 Gries, T. and Güde, H. (1999) Estimates of the nonconsumptive mortality of
631 mesozooplankton by measurement of sedimentation losses. *Limnol. Oceanogr.*, **44**, 459–465.
632 Gross, M. (2015) *Kernelheaping: kernel density estimation for heaped and rounded data*.
633 Freie Universitat Berlin.
634 Grossart, H. and Simon, M. (1998) Significance of limnetic organic aggregates (lake snow)
635 for the sinking flux of particulate organic matter in a large lake. *Aquat. Microb. Ecol.*, **15**, 115–125.
636 Håkanson, L. (1984) Suspension and calibration of a sediment trap. *Schweiz Z Hydrol.,* 46,
637 171–175.
638 Halfter, S., Cavan, E. L., Butterworth, P., Swadling, K. M., and Boyd, P. W. (2021)
639 "Sinking dead"—How zooplankton carcasses contribute to particulate organic carbon flux in the
640 subantarctic Southern Ocean. *Limnol. Oceanogr.*, lno.11971.
641 Johnston, S. E. Finlay, K., Spencer, R.G.M., Butman, D.E., Metz, M., Striegl, R., and
642 Bogard M.J. (2021) Zooplankton release complex dissolved organic matter to aquatic environments.
643 *Biogeochemistry*.
644 Kirillin, G., Grossart, H.-P., and Tang, K. W. (2012) Modeling sinking rate of zooplankton
645 carcasses: Effects of stratification and mixing. *Limnol. Oceanogr.*, **57**, 881–894.

Kolmakova, O., Gladyshev, M., Fonvielle, J., Ganzert, L., Hornick, T., and Grossart, H.-P. (2019) Effects of zooplankton carcasses degradation on freshwater bacterial community composition and implications for carbon cycling. *Environ. Microbiol.*, **21**, 34–49.

Koschel, R. and Adams, D. D. (2003) Preface: An approach to understanding a temperate oligotrophic lowland lake (Lake Stechlin, Germany). *Arch. Hydrobiol., Spec. Issues Advanc. Limnol.*, **58**, 1–9.

Kreling, J., Bravidor, J., Engelhardt, C., Hupfer, M., Koschorreck, M., and Lorke, A. (2017) The importance of physical transport and oxygen consumption for the development of a metalimnetic oxygen minimum in a lake: Metalimnetic oxygen minimum. *Limnol. Oceanogr.*, **62**, 348–363.

McCauley, E. (1984) The estimation of the abundance and biomass of zooplankton in samples. *A manual on methods for the assessment of secondary productivity in freshwaters*. Blackwell Sci. Publishers, London, pp. 228–265.

Moran, M. A. and Zepp, R. G. (1997) Role of photoreactions in the formation of biologically labile compounds from dissolved organic matter. *Limnol. Oeanogr.*, **42**, 1307–1316.

Neubauer, D., Kolmakova, O., Woodhouse, J., Taube, R., Mangelsdorf, K., Gladyshev, M., Premke, K., and Grossart, H.-P. (2021) Zooplankton carcasses stimulate microbial turnover of allochthonous particulate organic matter. *ISME J*, **15**, 1735–1750.

R Core Team (2021) *R: A language and environment for statistical computing*. R Foundation for Statistical Computing, Vienna, Austria.

Rojas-Jimenez, K., Araya-Lobo, A., Quesada-Perez, F., Akerman-Sanchez, J., Delgado-Duran, B., Ganzert, L., Zavialov, P. O., Alymkulov, *et al*. (2021) Variation of bacterial communities along the vertical gradient in Lake Issyk Kul, Kyrgyzstan. *Environ. Microbiol. Reports*, **13**, 337–347.

Scholtysik, G., Dellwig, O., Roeser, P., Arz, H. W., Casper, P., Herzog, C., Goldhammer T., Hupfer M. (2020) Geochemical focusing and sequestration of manganese during eutrophication of Lake Stechlin (NE Germany). *Biogeochemistry*, **151**, 313–334.

Schram, M. D. and Marzolf, G. R. (1994) Metalimnetic Oxygen Depletion: Organic Carbon Flux and Crustacean Zooplankton Distribution in a Quarry Embayment. *Transactions of the American Microscopical Society*, **113**, 105–116.

Selmeczy, G. B., Abonyi, A., Krienitz, L., Kasprzak, P., Casper, P., Telcs, A., Somogyvári, Z., Padisák J. (2019) Old sins have long shadows: climate change weakens efficiency of trophic coupling of phyto- and zooplankton in a deep oligo-mesotrophic lowland lake (Stechlin, Germany)—a causality analysis. *Hydrobiologia*, **831**, 101–117.

680 da Silva, A. J., de Melo, P. A. M. C., Neumann-Leitão, S., and de Melo Júnior, M. (2020)
681 Non-predatory mortality of planktonic copepods in a reef area influenced by estuarine plume.
682 *Marine Environmental Research*, **159**, 105024.
683 Simon, M., Grossart, H., Schweitzer, B., and Ploug, H. (2002) Microbial ecology of organic
684 aggregates in aquatic ecosystems. *Aquat. Microb. Ecol.*, **28**, 175–211.
685 Tang, K., Bickel, S., Dziallas, C., and Grossart, H. (2009) Microbial activities
686 accompanying decomposition of cladoceran and copepod carcasses under different environmental
687 conditions. *Aquat. Microb. Ecol.*, **57**, 89–100.
688 Tang, K. W., Backhaus, L., Riemann, L., Koski, M., Grossart, H.-P., Munk, P., and Nielsen,
689 T. G. (2019) Copepod carcasses in the subtropical convergence zone of the Sargasso Sea:
690 implications for microbial community composition, system respiration and carbon flux. *J. Plankton*
691 *Res.*, **41**, 549–560.
692 Tang, K. W., Hutalle, K. M. L., and Grossart, H. (2006a) Microbial abundance, composition
693 and enzymatic activity during decomposition of copepod carcasses. *Aquat Microb Ecol*, **45**, 219–
694 227.
695 Tang, K. W., Freund, C. S., and Schweitzer, C. L. (2006b) Occurrence of copepod carcasses
696 in the lower Chesapeake Bay and their decomposition by ambient microbes. *Estuarine, Coastal and*
697 *Shelf Science*, **68**, 499–508.
698 Tang, K. W., Gladyshev, M. I., Dubovskaya, O. P., Kirillin, G., and Grossart, H.-P. (2014)
699 Zooplankton carcasses and non-predatory mortality in freshwater and inland sea environments. *J.*
700 *Plankton Res.*, **36**, 597–612.
701 Tolomeev, A. P., Kirillin, G., Dubovskay, O. P., Buseva, Z. F., and Gladyshev, M. I. (2018)
702 Numerical Modeling of Vertical Distribution of Living and Dead Copepods Arctodiaptomus salinus
703 in Salt Lake Shira. *Contemp. Probl. Ecol.*, **11**, 543–550.
704 Tranvik, L. and Bertilsson, S. (2008) Contrasting effects of solar UV radiation on dissolved
705 organic sources for bacterial growth. *Ecology Letters*, **4**, 458–463.
706 Wetzel, R. G. (2001) *Limnology: lake and river ecosystems*. 3rd ed. Academic Press, San
707 Diego.
708 Wickham H., Averick M., Bryan J., Chang W., McGowan L.D., François R., Grolemund G.,
709 Hayes A., et al. Welcome to the tidyverse. Journal of Open Source Software, 4, 1686. doi:
710 10.21105/joss.01686.
711 Winslow, L., Read, J., Woolway, R., Brentrup, J., Leach, T., Zwart, J., Albers, S., and
712 Collinge, D. (2019) *rLakeAnalyzer: Lake Physics Tools*.
713 Wologo, E., Shakil, S., Zolkos, S., Textor, S., Ewing, S., Klassen, J., Spencer, R. G. M.,
714 Podgorski, D. C., *et al*. (2021) Stream Dissolved Organic Matter in Permafrost Regions Shows

715 Surprising Compositional Similarities but Negative Priming and Nutrient Effects. *Global*
716 *Biogeochem. Cycles*, **35**.
717 Yue, Y., Cai, L., Tang, Y., Zhang, Y., Yang, M., and Wang, F. (2021) Vertical Distribution
718 of Bacterial Community in Water Columns of Reservoirs With Different Trophic Conditions
719 During Thermal Stratification. *Front. Environ. Sci.*, **9**, 632089.

720 **Table and Figure legends**

721 Table 1. Average length, dry weight, biomass of live and dead zooplankton, sinking
722 velocities and normalized fluxes of dead cladocerans in Lake Stechlin. Significance of differences
723 in values between 7 m and 14 m were assessed by t-test.

724 Table 2. Average natural mortality rate, maximum carcass decomposition rates at 7 - 14 m,
725 and hypothetical sinking velocity at 14 m (model), corresponding to $D \approx 0$.

726 Fig. 1. Map of Lake Stechlin with sampling location.

727 Fig. 2. Example of calculated sinking velocity $v_{D0}(z)$ under the condition $D(z) \approx 0$ and
728 interpolated sinking velocity $v(z)$ by Equation 17 through the actual velocities determined via
729 sediment traps at 7 and 14 m depths for *Daphnia* on 1st August, 2017.

730 Fig. 3. Variations of vertical distributions of live and dead *D. cucullata*, variations of their
731 abundance per m^2 and the carcass sinking flux at 7 and 14 m as estimated via sediment traps.

732 Fig. 4. Variations of vertical distributions of live and dead *B. coregoni*, the variations of
733 their abundance per m^2 and carcass sinking flux at 7 and 14 m as estimated via sediment traps.

734 Fig. 5. Variations of vertical distributions of live and dead *D. brachyurum*, the variations of
735 their abundance per m^2 and carcass sinking flux at 7 and 14 m as estimated via sediment traps.

736 Fig. 6. Variations of vertical distributions of live and dead *C. sphaericus*, the variations of
737 their abundance per m^2 and carcass sinking flux at 7 and 14 m as estimated via sediment traps.

738 Fig. 7. Distributions (5-days averages) of live and dead *D. cucullata*, *B. coregoni*, and *D.*
739 *brachyurum* individuals and their corresponding fitted carcass sinking velocities (v) and degradation
740 rates (D).

741 Fig. 8. Vertical distribution of total biomass of live and dead *D. cucullata*, *B. coregoni*, and
742 *D. brachyurum* in Lake Stechlin (27th July to 1st August, 2017), as well as their corresponding
743 model calculations of LOM release into the water column as I_{DWp} and I_D and their sum.
744

745 Table 1

Parameter	*D. cucullata*	*B. coregoni*	*D. brachyurum*	*C. sphaericus*
Length (mm) ± SE	0.714 ± 0.010	0.430 ± 0.006	0.723 ± 0.008	0.267 ± 0.003
Dry weight DW (µg) ± SE	1.91 ± 0.072	1.92 ± 0.068	1.35±0.043	0.78 ± 0.032
Biomass and percent contribution in cladoceran biomass (mg m^{-2})	566.67 ± 45.8 (49.71%)	101.44 ± 15.48 (8.9%)	345.61 ± 44.97 (30.32%)	126.29 ± 6.99 (11.08%)
Percentage of dead of each species	4.82 ± 0.48 %	8.91 ± 0.89 %	5.85 ± 0.88 %	4.59 ± 0.43 %
Measured sinking velocities *v*, m d^{-1}				
7 m	2.15 ± 0.40	14.01 ± 0.98	1.10 ± 0.20	*17.52 ± 2.40*[a]
14 m	7.64 ± 1.62	19.53 ± 1.92	5.88 ± 1.44	9.31 ± 1.31
t-test	**3.30**	**2.55**	**3.28**	-
Normalized flux $\bar{F}$, d^{-1}				
7 m	0.007 ± 0.001	0.134 ± 0.011	0.017 ± 0.004	-
14 m	0.006 ± 0.001	0.110 ± 0.009	0.003 ± 0.001	-
Percentage of flux reduction between water layers	14.3%	17.9%	82.3%	
t-test	0.94	1.72	**3.43**	-

746 [a] artifact of sinking velocity determination (*C. sphaericus*) at 7 m, explanation provided in the main text. Bolded t-
747 values represent significant differences ($p < 0.05$)

748

749 Table 2.

Fitted parameters	*D. cucullata*	*B. coregoni*	*D. brachyurum*
m – specific mortality rate (d^{-1})	0.008 ± 0.001	0.129 ± 0.012	0.020 ± 0.004
D_{max} – maximum specific destruction rate of carcasses in the layer 0 – 14 m (d^{-1})	0.362 ± 0.076	0.709 ± 0.263	3.990 ± 1.109
Hypothetic sinking velocities (m d^{-1}) at 14 m depth, calculated for the case D ≈ 0	11.8 ± 1.9	23.7 ± 3.6	34.9 ± 9.5
Ratio of hypothetical sinking velocity (for D ≈ 0) to observed one at 14 m	1.5	1.2	5.9
Contribution of species to total LOM (mg DW m^{-2}) $I_{DW\rho}$ - fraction	2.18 ± 0.13 (25.6 %)	3.87 ± 0.42 (44.3 %)	2.6 ± 0.32 (30.1 %)
I_D - fraction	0.54 ± 0.15 (10.1 %)	1.57 ± 0.61 (27.5 %)	2.93 ± 0.54 (62.4 %)

750

751

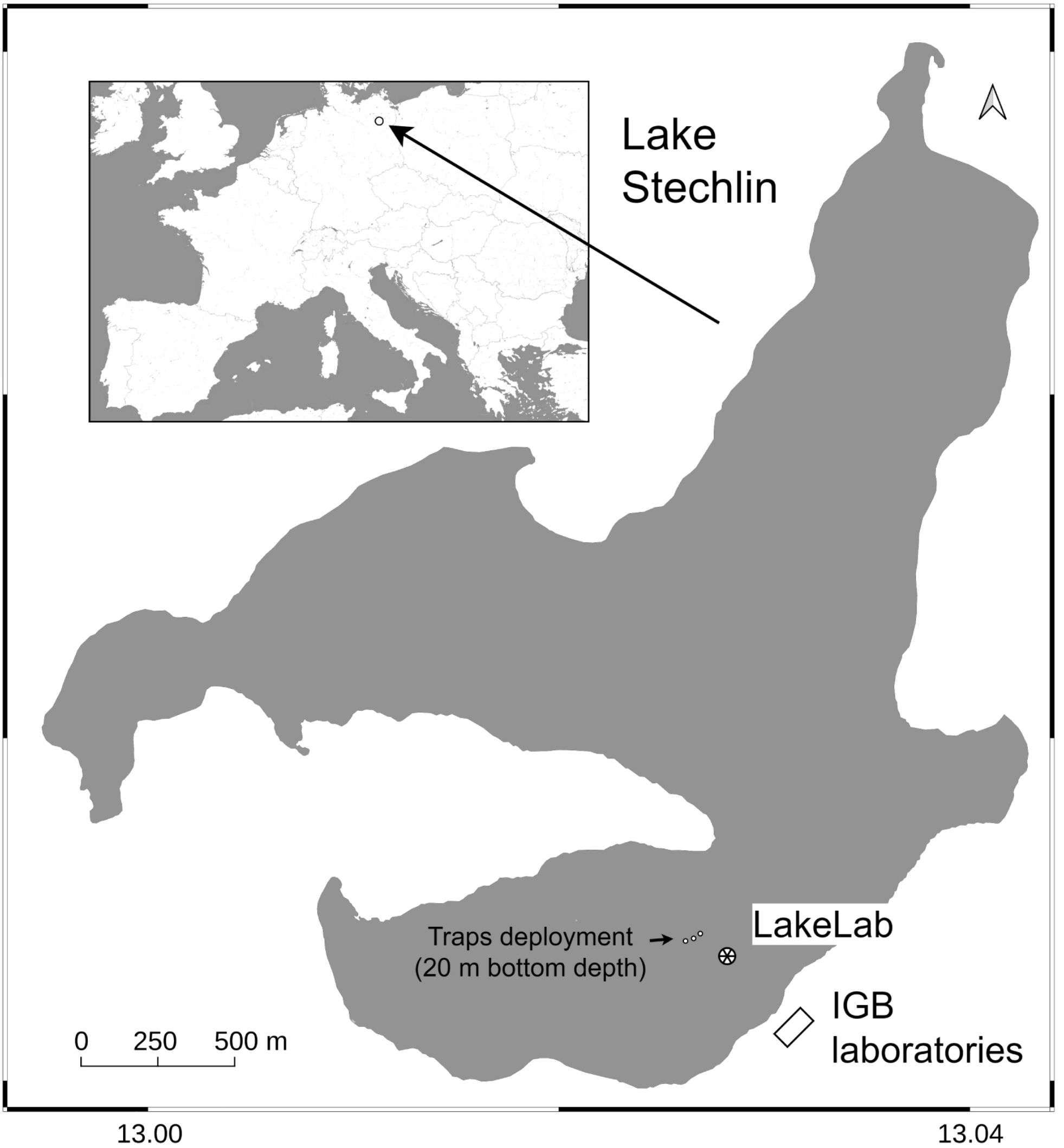
Lake
Stechlin
Traps deployment
(20 m bottom depth)
LakeLab
IGB
laboratories
0 250 500 m
53.16
53.14
13.00
13.04

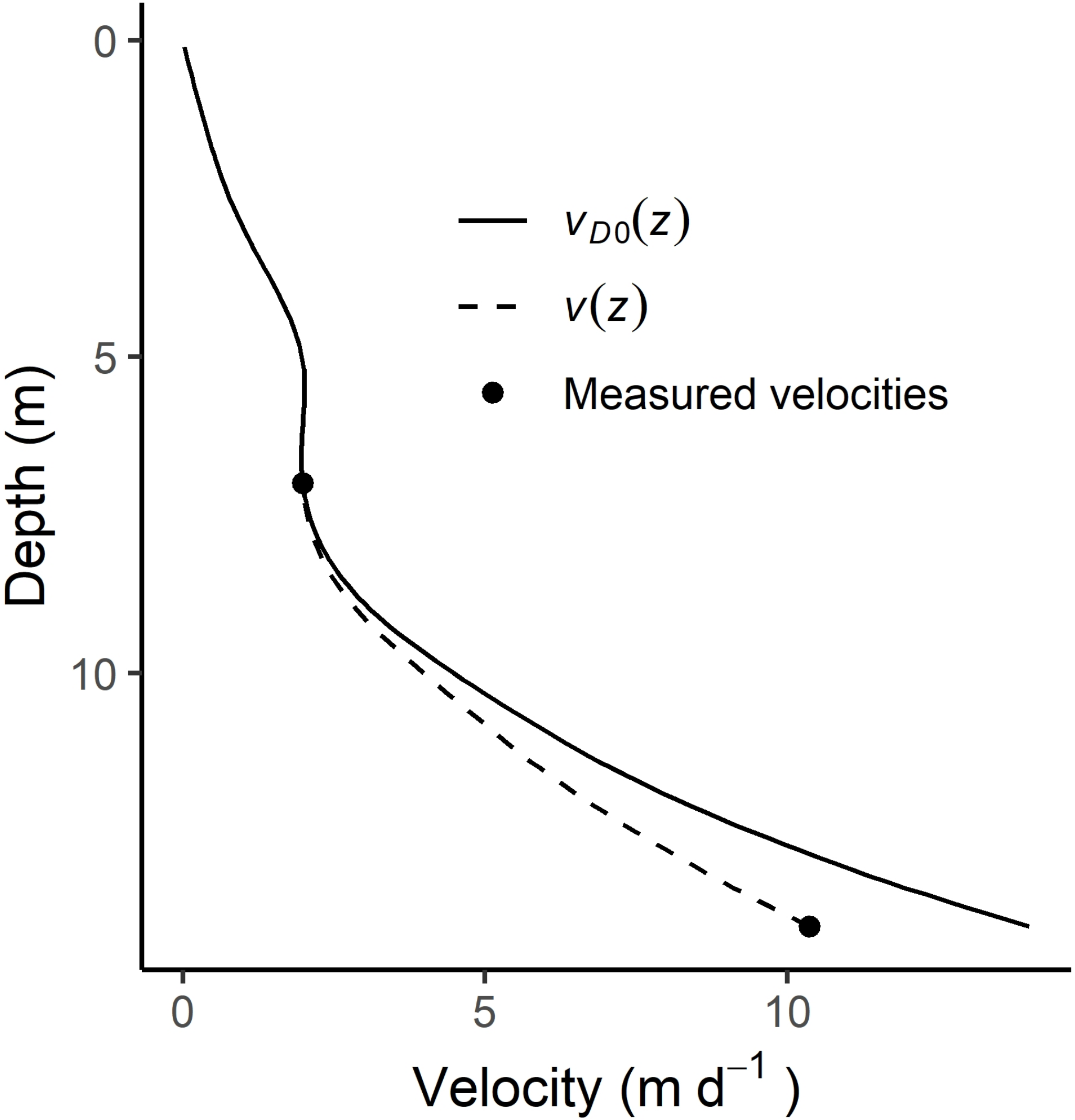
0
5
10
Depth (m)
$v_{D0}(z)$
$v(z)$
Measured velocities
0
5
10
Velocity (m d^{-1})

Daphnia cucullata

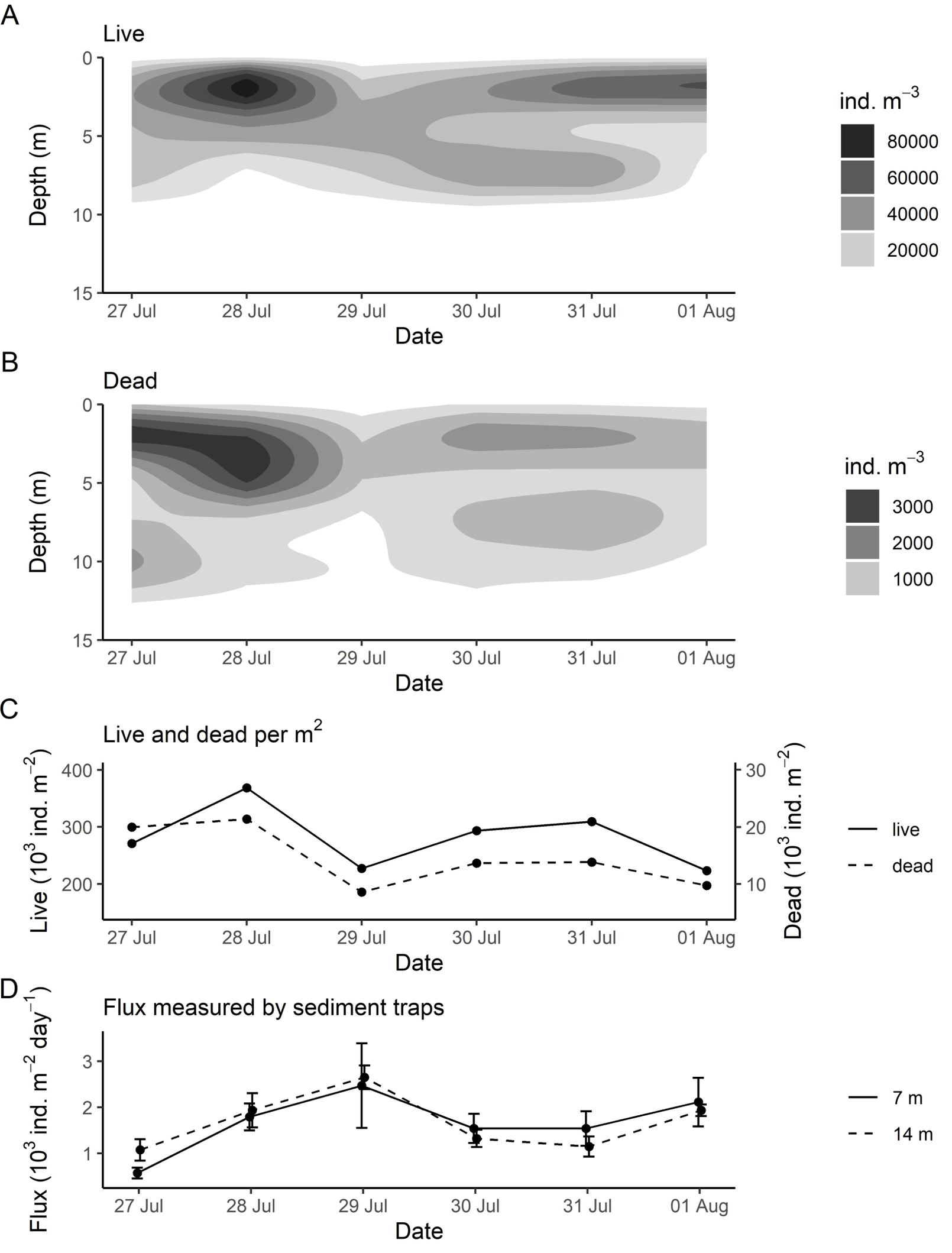

Bosmina coregoni

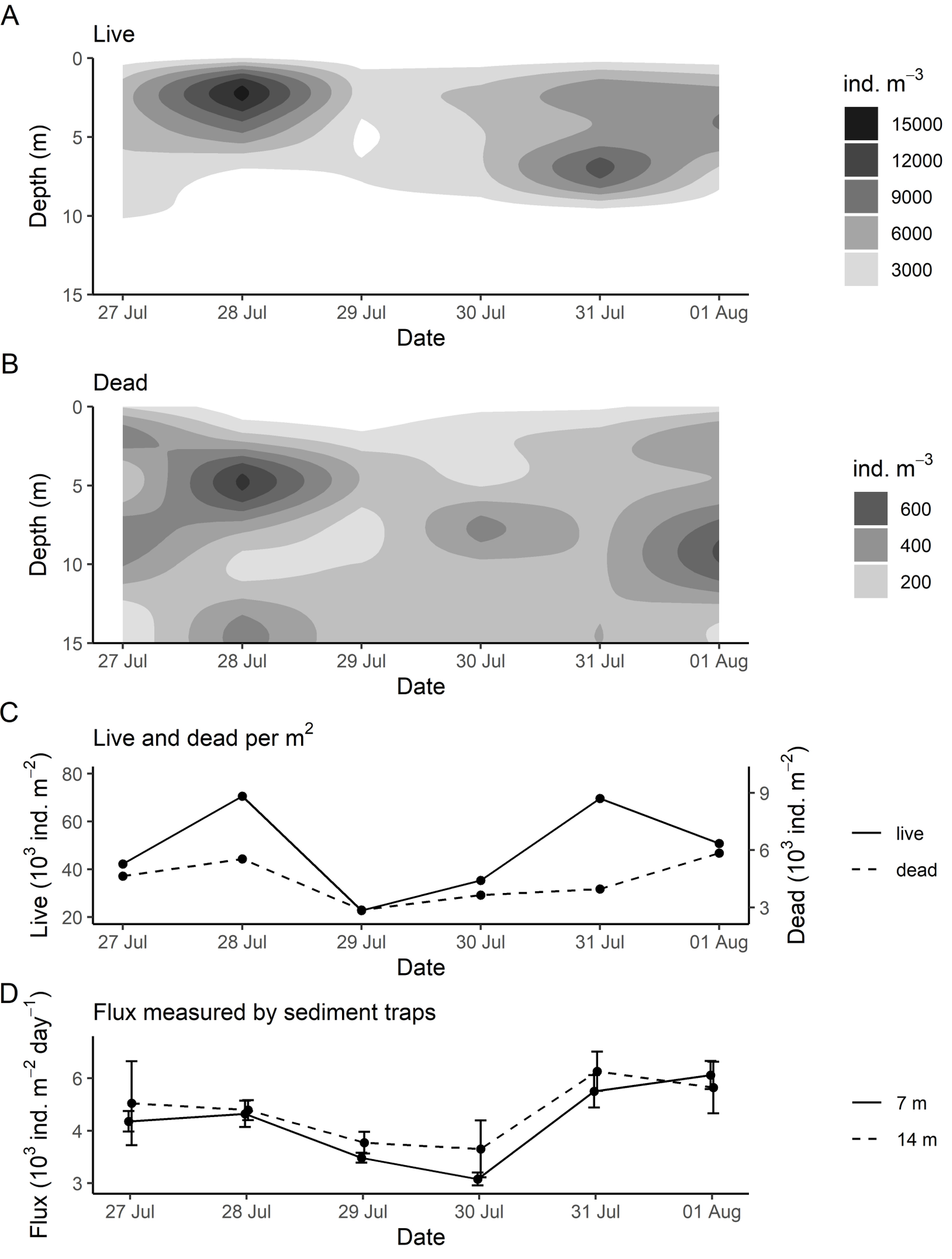

Diaphanosoma brachyurum

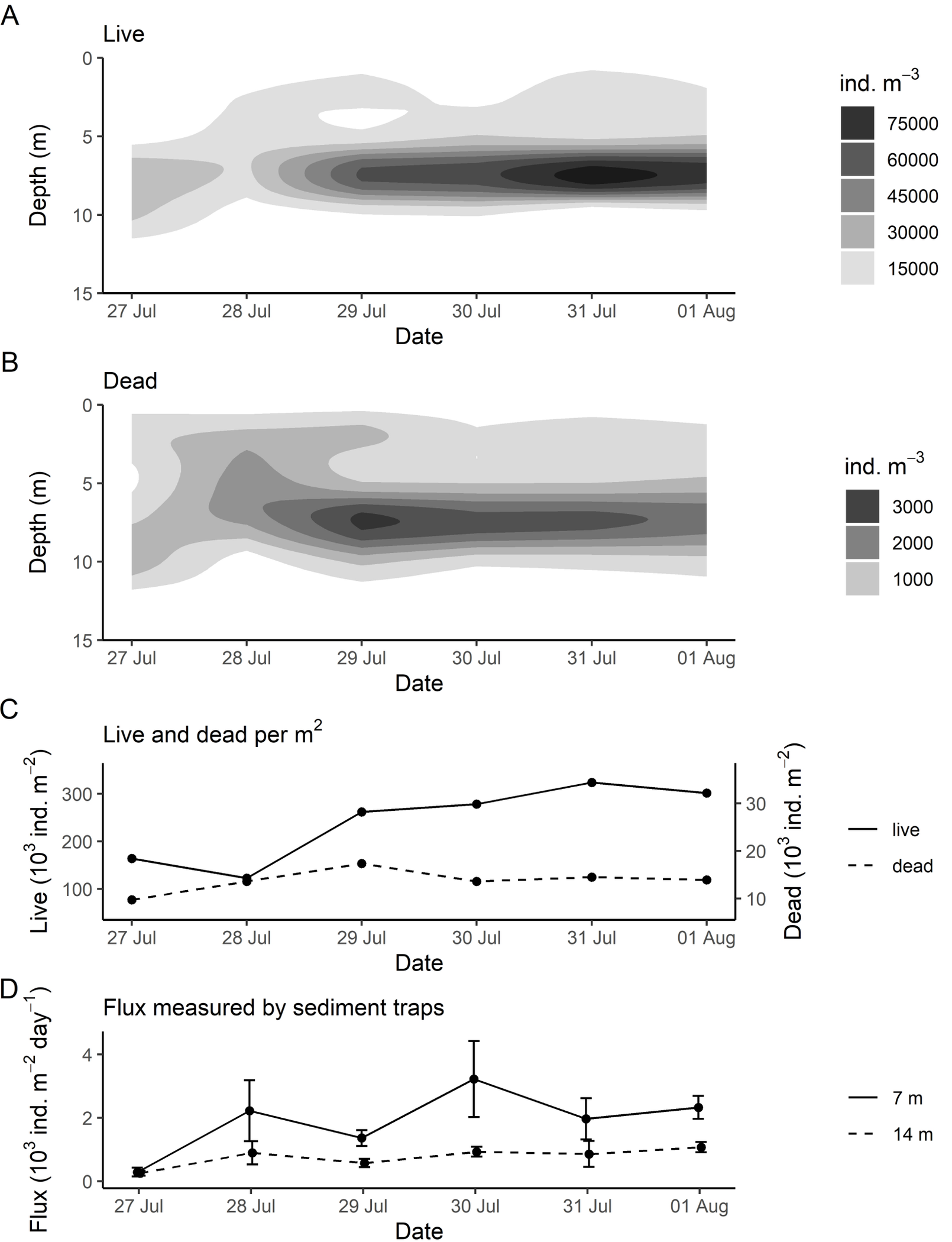

Chydorus cf. sphaericus

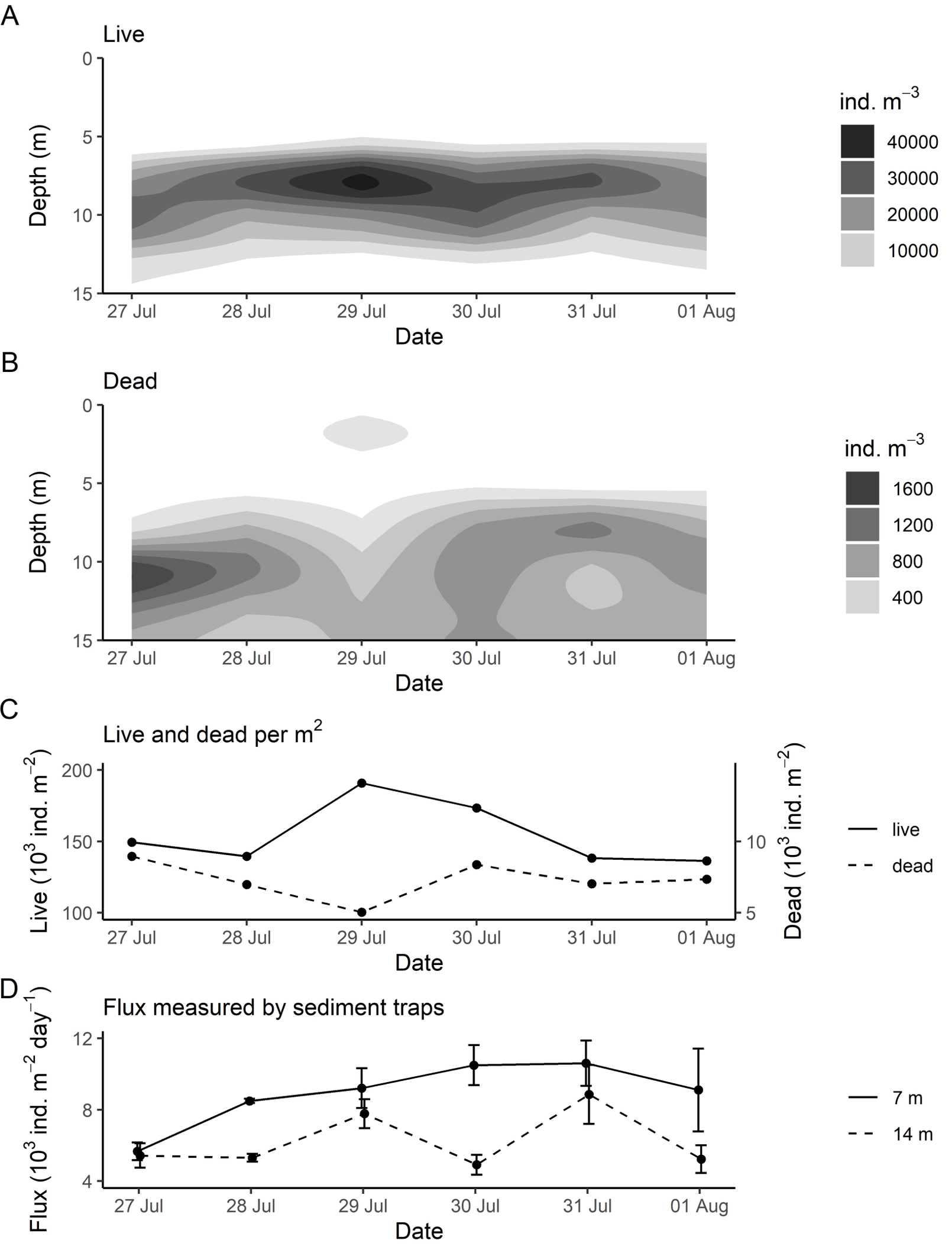

Daphnia cucullata

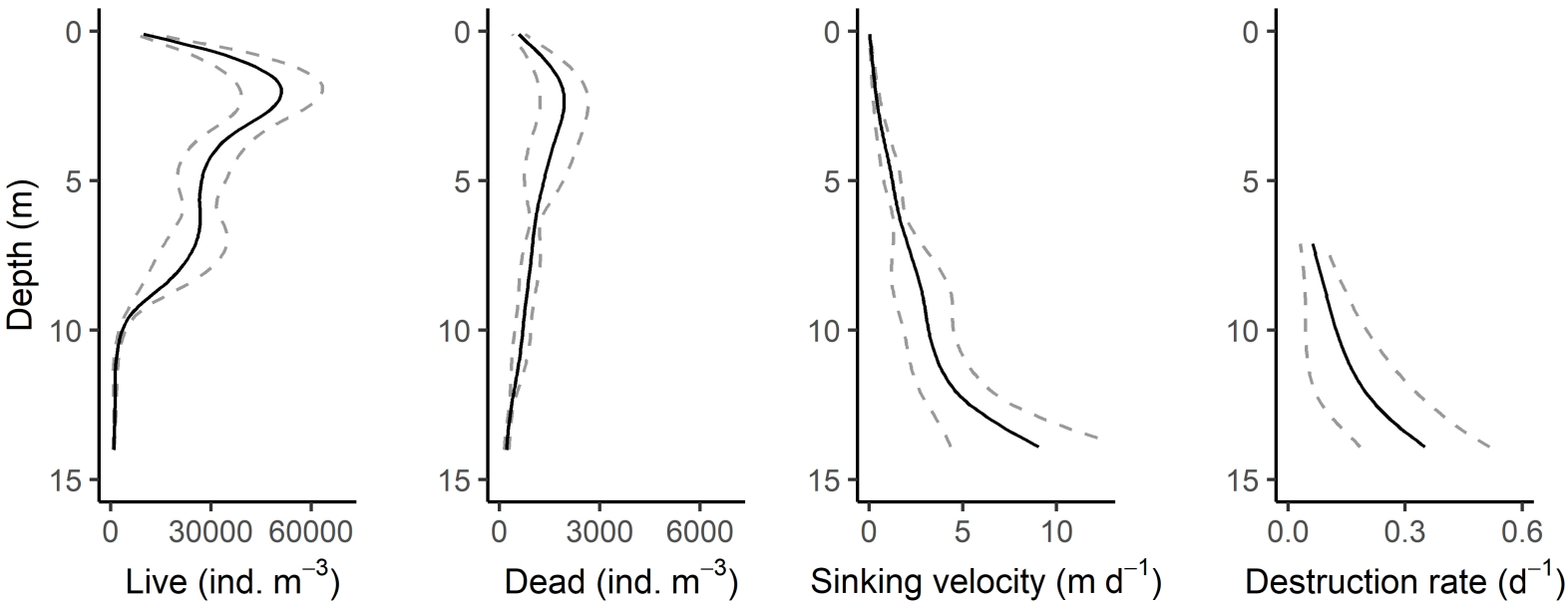

Bosmina coregoni

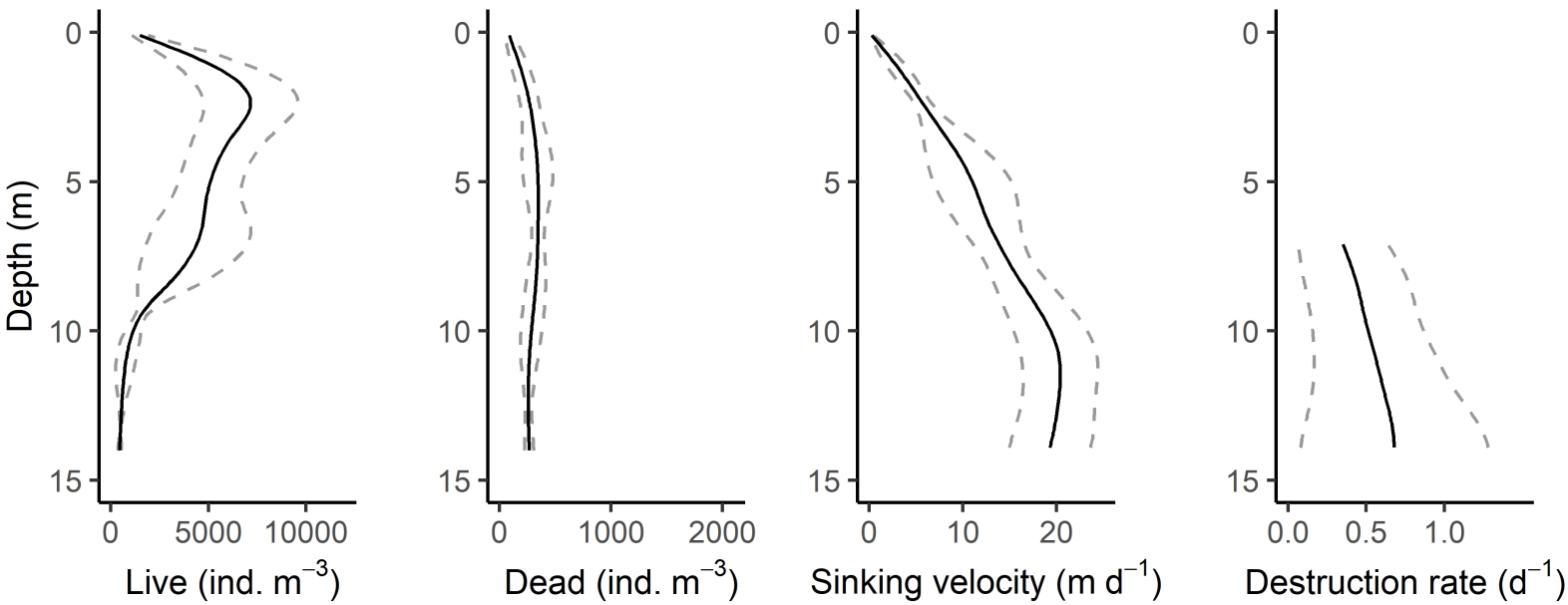

Diaphanosoma brachyurum

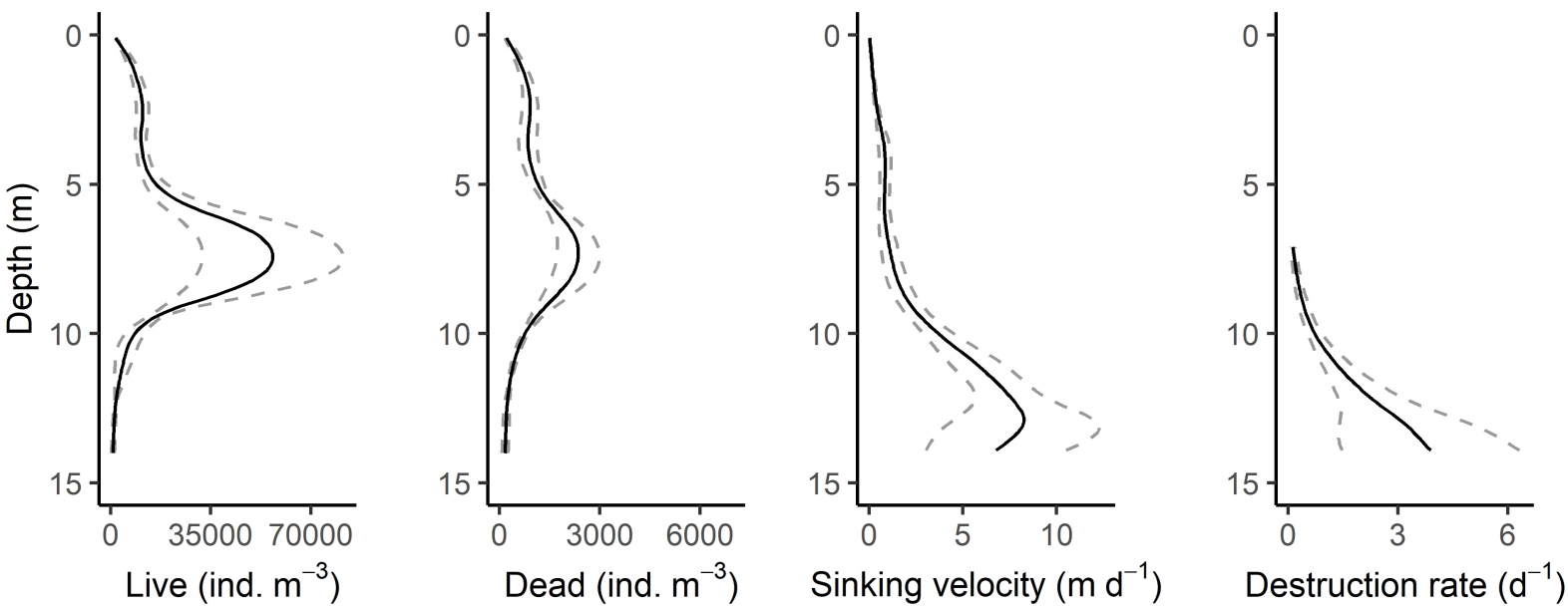

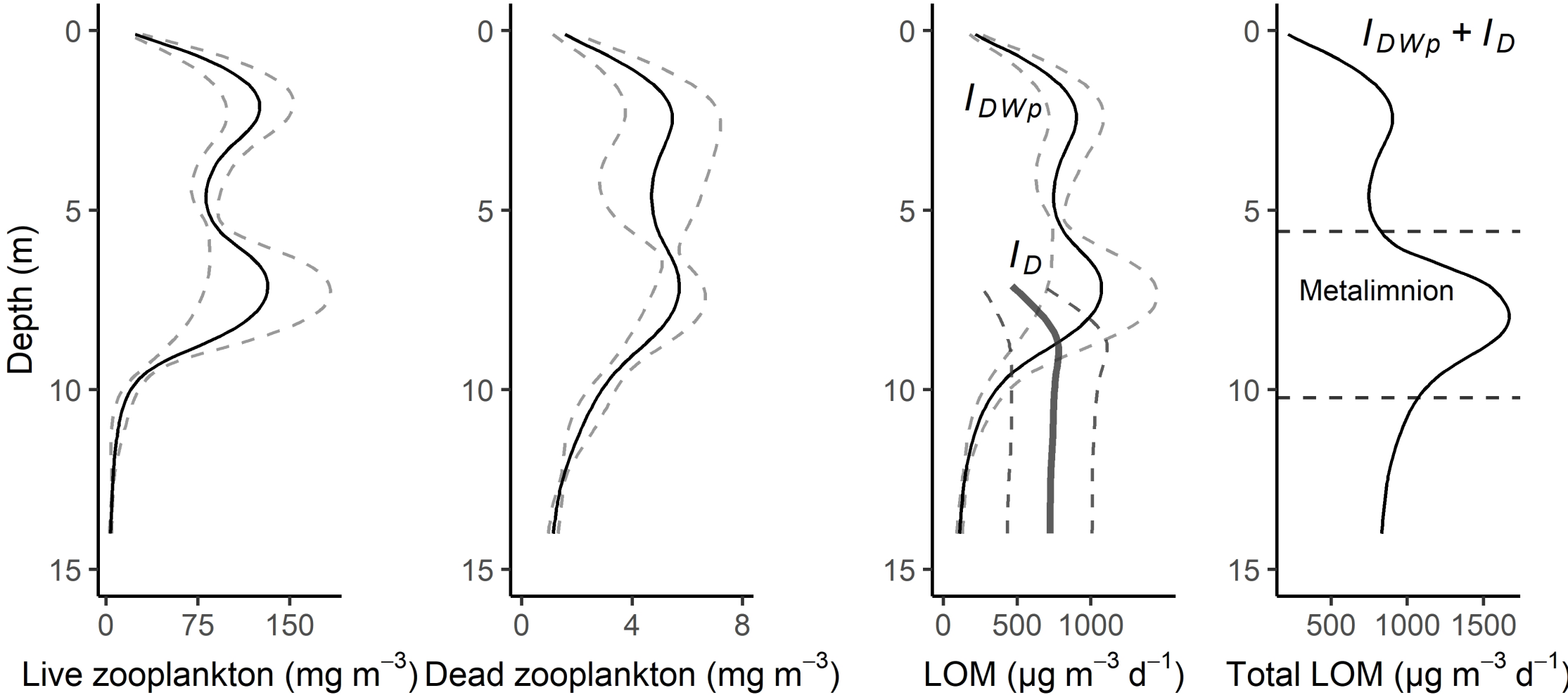
Depth (m)
0
5
10
15
0
75
150
Live zooplankton (mg m^{-3})
0
4
8
Dead zooplankton (mg m^{-3})
I_{DWp}
I_D
0
500
1000
LOM (µg m^{-3} d^{-1})
$I_{DWp} + I_D$
Metalimnion
500
1000
1500
Total LOM (µg m^{-3} d^{-1})